

# RatBodyFormer: Rodent Body Surface from Keypoints

Ayaka Higami<sup>1</sup> Karin Oshima<sup>2</sup> Tomoyo Isoguchi Shiramatsu<sup>2</sup>  
Hirokazu Takahashi<sup>2</sup> Shohei Nobuhara<sup>3</sup> Ko Nishino<sup>1</sup>

<sup>1</sup> Graduate School of Informatics, Kyoto University

<sup>2</sup> Graduate School of Information Science and Technology, The University of Tokyo

<sup>3</sup> Faculty of Information and Human Sciences, Kyoto Institute of Technology

<https://vision.ist.i.kyoto-u.ac.jp/research/ratbodyformer/>

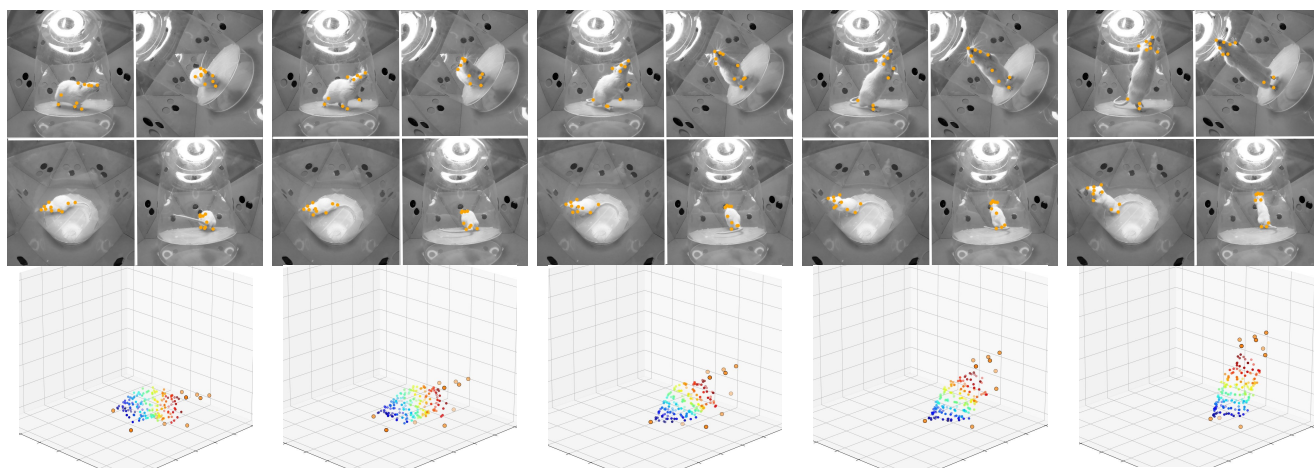


Figure 1. We introduce a novel multiview camera system (RatDome) to capture multiview videos of rats (top), and a novel Transformer-based network (RatBodyFormer) that learns to predict dense body surface points of a rat from its detectable keypoints from large-scale data (RatDome Dataset) captured with it (bottom). Past methods predict only sparse 2D keypoints such as their faces and legs (orange points). Our RatBodyFormer turns them into the dense 3D body surface (colorful points) offering a much richer window into the complex rat behavior.

## Abstract

*Rat behavior modeling goes to the heart of many scientific studies, yet the textureless body surface evades automatic analysis as it literally has no keypoints that detectors can find. The movement of the body surface, however, is a rich source of information for deciphering the rat behavior. We introduce two key contributions to automatically recover densely 3D sampled rat body surface points, passively. The first is RatDome, a novel multi-camera system for rat behavior capture, and a large-scale dataset captured with it that consists of pairs of 3D keypoints and 3D body surface points. The second is RatBodyFormer, a novel network to transform detected keypoints to 3D body surface points. RatBodyFormer is agnostic to the exact locations of the 3D body surface points in the training data and is trained with*

*masked-learning. We experimentally validate our framework with a number of real-world experiments. Our results collectively serve as a novel foundation for automated rat behavior analysis and will likely have far-reaching implications for biomedical and neuroscientific research.*

## 1. Introduction

Rodent behavior analysis underpins the scientific process of many areas in biomedical and neuroscientific research. The behavioral outcomes of rodents play a key role in validating hypotheses that lead to scientific discoveries. Careful observations of rodent behaviors, however, incur cost in manpower and time, causing a bottleneck in the scientific process. Human observation is also prone to errors. Subtle be-

havioral differences may be missed or misjudged [9, 31]. If we can automate this experimental validation process while ensuring its accuracy or even extend it beyond the human level, we may dramatically expedite the scientific discovery process [8, 12, 15, 33]. For instance, it would enable concurrent testings of many hypotheses.

We focus on rats, the most commonly used rodent in scientific experiments. A growing number of recent works, indeed, target computational rat behavior analysis or provide the basis for it. Belongie *et al.* [2] pioneered rat tracking by modeling the whole body as a spatio-temporal blob. Chaumont *et al.* [7] refined the method by dividing each blob into three parts linked with physical constraints. More recently, Mathis *et al.* [1] introduced a pre-trained deep network that can be fine-tuned to extract 2D keypoints of interest. This provides a general framework for skeleton estimation of animals, very much in the spirit of human pose estimation [6].

These past methods, however, only provide us with the means to understand rat behavior through the movements of sparse keypoints. With DeepLabCut [1], trackable points of a rat would typically lie on the face, hands, feet, and tail. Although the movements of these keypoints may suffice for a range of applications, for instance, to recognize when a rat is feeding itself, they only give a sparse sampling of the entire body which tells us much less than what the detailed movements of other body parts may convey.

The largest missed opportunity lies in the body surface, the fur-coated elastic body that shows subtle twitches, twists, curl-up, stretching, and even hair standing which all eloquently speak to the rich inner conditions of the rat and colorize their behavior with context. Missing the body surface is inevitable with a keypoint-based method, even with large-scale pre-training, as the rat body lacks any texture whatsoever for such keypoint detectors to latch on to. It is just a uniform white or dark-brown surface. It is also highly non-rigid and deformable, much more so than the human body. At the same time, even though the rats are the same at the DNA level, their body surfaces can be slightly different in size and shape across different ages in months.

How then can we model the 3D body surface of rats? Our goal is to realize full 3D rat reconstruction including the body surface without interfering with its natural behavior. We achieve this by learning to recover the 3D body surface from the handful of keypoints that can be automatically detected. Our key idea is to learn and leverage the coordination between the well-defined keypoints and the non-rigid movements of the body surface.

We make two key technical contributions for this. The first is a novel means to collect training data. We need a sizable amount of training data that associates representative keypoints including facial features and appendages with densely sampled points of the body surface. The rat body surface is textureless and deformable, to the point that it is

near impossible even for a human to annotate. We overcome this by temporarily attaching trackable points (colorful beads) and passively capturing them in a novel multi-camera system which we refer to as the RatDome. We show that we can automatically recover the keypoints together with the 3D body surface points at each time instance with multiview geometry. We call this first-of-its-kind dataset, the RatDome dataset. The second is a novel network to transform detected 3D keypoints to 3D body surface points. We realize this with a transformer-based model that is agnostic to the exact locations of the 3D body surface points in the training data and introduce masked-learning to train it. We refer to this model as RatBodyFormer.

We experimentally validate our framework with a number of real-world experiments using rats for neuroscientific studies. We first show that our RatBodyFormer can estimate the body surface accurately regardless of their poses or shapes. Our model can estimate their body surface with an average L2 error of around 6mm, approximately the same diameter as the beads attached to the body surface. We also show that rat body movements can be predicted by simply forecasting the keypoints from their past movements. This may help better segregate the movements of multiple rodents and serve as a useful tool to understand their interactions. We believe our RatDome dataset and RatBodyFormer offer foundational tools for advancing the automation of rodent behavior analysis and together open a new avenue of research towards computer vision for science.

## 2. Related Work

**Rodent Behavior Analysis** Many methods have been proposed for automatic rodent behavior modeling [32, 36, 37]. Mimica *et al.* [36] reproduced human mocap on rats with retroreflective markers. Maghsoudi *et al.* [32] painted markers on the rat body and tracked them based on their colors. These methods are invasive and can lead to significantly altered behaviors as they require markers on the rat body in the actual experiments.

Markerless, non-invasive methods have also been proposed [2, 5, 7, 35]. Belongie *et al.* [2] introduced a detection and tracking method for a mouse using spatio-temporal volumes of monocular video. Matsumoto *et al.* [35] tracked major body parts (head, neck, trunk, and hip) with 3D skeleton estimation with depth sensing.

More recently, deep learning based keypoint detection has become popular [1, 3, 10, 14, 19, 39, 46, 48]. DeepLabCut [1] detects manually specified keypoints through transfer learning of 2D human pose estimation from monocular images [40]. DANNCE [10] and FreiPose3D [48] similarly apply human pose estimation and integrate multiview images to estimate 3D keypoints. LiftPose3D [14] achieves monocular 3D animal pose estimation by leveraging a deep neural network for lifting 2D human poses to 3D [34].

All these methods only detect sparse keypoints such as facial points and paws and cannot be applied to the featureless body surface [11]. Our method complements these methods by establishing a framework to extrapolate dense points of the textureless body surface from feature-rich keypoints completely noninvasively without any markers.

**3D Animal Reconstruction** One common approach for 3D human reconstruction is to learn a statistical model from pre-acquired 3D scans to better condition the solution space [28, 30, 49, 51]. SMPL [30] is a statistical 3D human linear blended shape model parameterized by the person’s shape and pose. The pose parameters are the joint rotations and the shape parameters are the PCA coefficients of a large collection of aligned body scans. SMAL [49] extends this to quadrupled animals. Most 3D reconstruction methods regress these parameters directly from the image with a neural network [23, 47] or optimize their parameters so that projected keypoints align with their imaged ones [4, 20, 21, 25]. Joints of rodents are, however, not well-defined as they are deeply veiled by their fluffy body. Instead, we leverage reliably detectable 3D keypoints to recover the body surface.

Recent works have also introduced image-based animal appearance modeling [29, 42, 45, 50]. AnimalAvatars [42] regresses continuous surface embedding [38] from an image to associate each pixel with a point on the target 3D shape in its canonical pose. This CSE estimation, however, requires large-scale dense annotation between 2D image pixels and a 3D canonical surface ala DensePose [16], which is costly and unreliable for textureless body surfaces. In contrast, we leverage beads and multiview geometry to learn the sparse keypoint to dense body surface mapping, which ensures positional consistency and robust mapping.

### 3. Method

We learn to estimate the rat body surface from its detected keypoints. First, we collect a dataset that associates densely sampled body surface points with detectable keypoints with a newly developed multiview camera system which we refer to as the RatDome (Sec. 3.1). Second, we derive a transformer-based network that takes the keypoint 3D coordinates as input and outputs sampled body surface point 3D coordinates. We refer to this network as RatBodyFormer (Sec. 3.2). The model is trained with the data collected with RatDome (RatDome Dataset).

The experimental protocol of this study received approval by the Committee on the Ethics of Animal Experiments at the Graduate School of Information Science and Technology at the University of Tokyo (Permit Number: JA23-6).

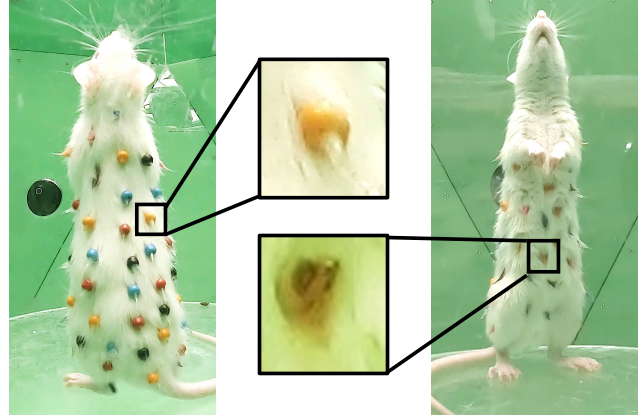


Figure 2. A color-beaded rat. We attach color (red, black, orange, blue) beads (left) and paint on the rat body surface (right).

#### 3.1. RatDome Dataset

Regardless of the pre-training, a network can only learn to detect points that exhibit sufficient visual features. As a result, even after fine-tuning, an off-the-shelf deep keypoint detector [1] can only reliably detect points on the face and appendages of the rat. Our goal is to learn to extrapolate the body surface from these keypoints. For this, we will need a sufficiently large-scale dataset of paired sets of 3D keypoints and 3D body surface points. This is challenging as the rat body is completely textureless.

We overcome this challenge by simply endowing the rat with body texture. As shown in Fig. 2, we attach color beads to the body as well as paint markers in the areas where beads cannot be attached. We refer to these two types of body markers, beads and paints, simply as *markers*. It is important to note that these markers are only used for training data capture and the rats are completely in their natural form when their behavior is observed in actual experiments. These markers are also small enough that they do not alter the rat’s behavior as far as we could tell.

We build a novel multi-camera system to passively observe the color-beaded rat and reconstruct the 3D coordinates of individual markers. As shown in Fig. 3, this RatDome is a rat-scale multiview studio. Its shape is a gyroelongated pentagonal pyramid with 15 faces. Each face is an equilateral triangle with sides of 400mm, and accommodates up to three cameras or microphones on it while also serving as a green background of the system. For our data capture, we mount one camera on each face totaling 15 views. RatDome follows the modular design of CMU Panoptic studio [22] and can adapt to new capture devices by replacing each face.

By capturing freely moving rats of different ages (7, 9, 11 week-old) in RatDome, we collect multiview videos and the paired sets of 3D keypoints and 3D markers. We

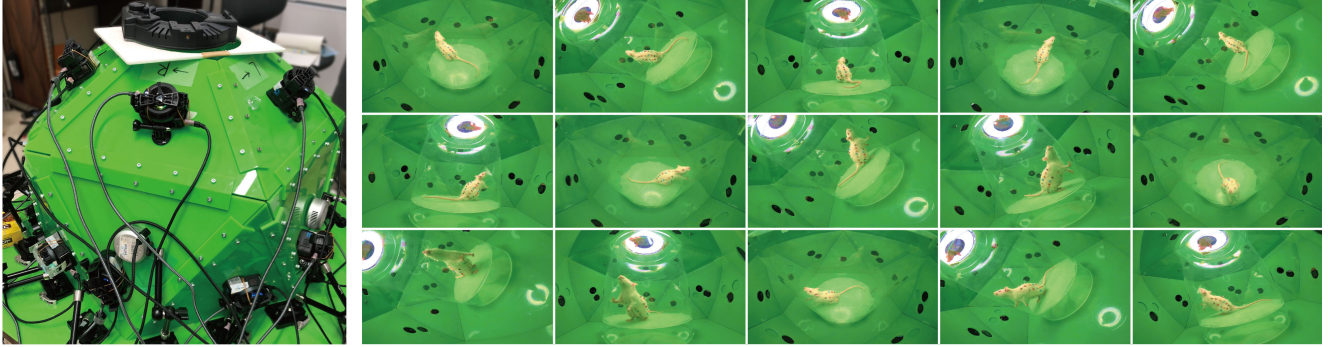


Figure 3. RatDome is a novel multiview camera studio for freely moving rats. It is shaped as a 15-faced gyroelongated pentagonal pyramid. With 15 cameras and their multiview geometry, we collect, annotate, and reconstruct paired sets of 3D keypoints and 3D body surface points of rats of different ages in weeks.

recorded 2 sessions for the 7 week-old, 1 session for the 9 week-old, and 2 sessions for the 11 week-old. Each session was approximately 10 to 15 minutes. We manually annotate the marker IDs for the 7 and 11 week-old rats for about 1100 frames each. We semi-automatically annotate (see Sec. 3.2) the 7, 9, and 11 week-old rats’ marker IDs for about 8000, 1900, and 10000 frames, respectively. The 7, 9, 11 week-old rats have 58, 37, and 66 surface markers, respectively. We refer to this first-of-its-kind large-scale rat body surface dataset as the *RatDome Dataset*.

A notable difference of the RatDome Dataset from other datasets used for building parametric 3D shape models [30, 49, 51] is that the marker positions across different individuals are not consistent as it is impossible to make them the same. Although the marker positions are the same within a single rat for multiple capture sessions, it is not strictly aligned for different rats. In other words, our RatDome Dataset can be seen as a collection of multiple motion captures each of which has slightly different annotations, similarly to the SuperAnimal dataset [46]. This means that we cannot just apply PCA to obtain a universal statistical model [30, 49, 51].

### 3.2. RatBodyFormer

The markers in RatDome Dataset are not consistent across individual rats and the body surface deforms non-rigidly depending on the pose. To model this highly nonlinear deformation with inconsistent annotations, we derive a novel transformer-based model (RatBodyFormer) to recover dense 3D body surface points from sparse keypoints.

**Model Formulation** RatBodyFormer takes  $K$  3D keypoint coordinates as input and outputs  $N$  3D surface point coordinates. The keypoints are chosen as points locatable in images, and we use the following 10 points: *nose, right and left eyes, ears, front paws, back paws, and the base of tail*. We use these in lieu of body joints, *e.g.*, shoulders, since

the body joints are ill-defined from the appearance of a rat unlike humans or horses [30, 49, 51].

As shown in Fig. 4, RatBodyFormer is designed as a Transformer encoder-decoder model [44]. Each encoder input token represents each keypoint, and each decoder output token represents each body surface point.

**Canonical 3D Body Surface** To consolidate annotations based on different marker positions, RatBodyFormer employs a canonical body surface  $\tilde{S}$  onto which all markers are mapped. We pre-select a reference pose that appears multiple times in the captured sequences. By using the 3D keypoint positions as the deformation constraint, we can align all the individually observed 3D surfaces for that pose with ARAP deformation [43]. This brings all marker positions for this reference pose to a single surface.

In our RatDome Dataset, we manually selected a standing-on-two-feet pose as shown in Fig. 2 as the reference pose such that almost all of the whole body surface is visible from the cameras. Please refer to the appendix for details. As a result, the keypoints and the surface points are associated with 3D points on  $\tilde{S}$  as  $\tilde{\mathbf{P}} = \{\tilde{p}_i\}_1^K$  and  $\tilde{\mathbf{B}} = \{\tilde{b}_j\}_1^N$ , respectively.  $\tilde{\mathbf{P}}$  and  $\tilde{\mathbf{B}}$  are constant regardless of the body shape and pose.

**Network Architecture** To represent different body shapes of different rats, we introduce point-wise scaling and translation parameters for individual rat,  $\mathbf{C}_P = \{c_{p_i}\}_1^K$ ,  $\mathbf{T}_P = \{t_{p_i}\}_1^K$  and  $\mathbf{C}_B = \{c_{b_j}\}_1^N$ ,  $\mathbf{T}_B = \{t_{b_j}\}_1^N$  for keypoints and body surface points, respectively. These scaling and translation parameters are optimized in the training process. At inference time for a rat whose scaling and translation parameters are unknown, we test-time optimize the parameters while keeping RatBodyFormer frozen.

The keypoints and the body surface points are first rotated around the Z-axis, *i.e.*, the direction of gravity, such that the rat face is oriented to a pre-determined direction. Their 3D coordinates are then normalized to  $[-1 : 1]$ :

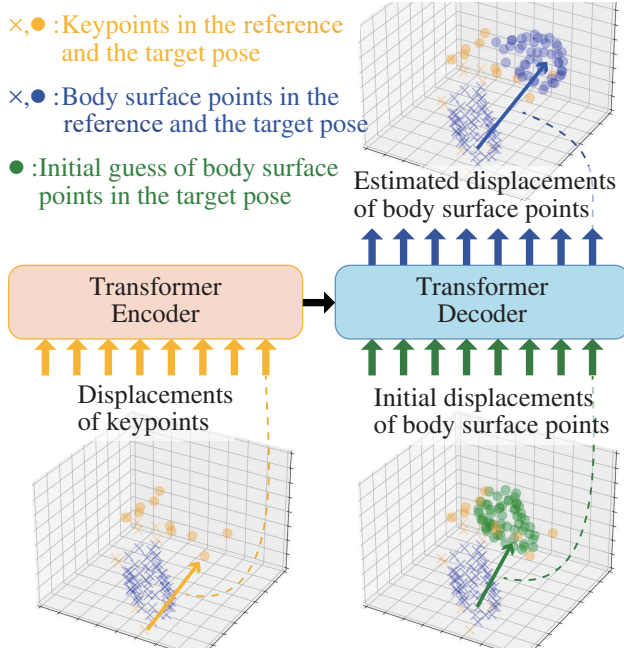


Figure 4. RatBodyFormer is an encoder-decoder Transformer model that takes the normalized displacements of detected 3D keypoints and outputs the normalized displacements of densely sampled 3D body surface points. The displacements are with respect to the reference pose.

$\mathbf{P} = \{p_i\}_1^K$  and  $\mathbf{B} = \{b_j\}_1^N$ . The same normalization is also applied to  $\tilde{S}$ .

As shown in Fig. 4, the decoder outputs are the estimated normalized displacements of the body surface points from their coordinates in the reference pose. The decoder queries are normalized displacements of the body surface points in an initial guess  $\tilde{\mathbf{B}}$  from their coordinates in the reference pose. The initial guess is calculated analytically. We use ARAP [43] and deform  $\tilde{S}$  with the constraint that  $\tilde{\mathbf{P}}$  is aligned with  $\mathbf{P}/C_P$ . As a result, we obtain the ARAP-deformed  $\tilde{\mathbf{B}}$  as  $\tilde{\mathbf{B}} = \{\tilde{b}_j\}_1^N$ . For each keypoint and body surface point, we use the displacement vector normalized by the identity-dependent parameters  $p_i/c_{p_i} - (\tilde{p}_i + t_{p_i})$  and  $\hat{b}_j/c_{b_j} - (\tilde{b}_j + t_{b_j})$  as the inputs to the model, respectively.

The encoder and the decoder first embed each of these displacements in higher dimension  $d$  together with positional encoding. The positional encoding for keypoints and body surface points is defined with a set of sinusoidal functions of the projection of their positions  $\tilde{p}_i$  and  $\tilde{b}_j$  on  $\tilde{S}$  by the Laplace-Beltrami eigenfunctions defined on the canonical body surface  $\tilde{S}$  [27, 38]. The output of the RatBodyFormer decoder are  $N$  normalized displacement vectors  $\{\delta_j\}_1^N$ . Each  $\delta_j$  reconstructs the body surface coordinates as  $c_j(\delta_j + \tilde{b}_j + t_{b_j})$ . We set  $d = 128$  in the experiment.

**Loss Functions** The primary loss function for training RatBodyFormer is the supervision provided by the annotations in the RatDome Dataset. We directly compare the estimated 3D body surface point coordinates and their ground-truth coordinates with L2 norm as  $\mathcal{L}_{3D}$ . This L2 norm loss  $\mathcal{L}_{3D}$ , however, can be defined only for a subset of the  $N$  body surface points. Since they are defined as the union of all annotated body surface points on different rat surfaces, a single input keypoint set from a rat has a ground-truth annotation only for the body surface points of the same rat. Even for the body surface points from the same rat, some of them can be missing in the captured data due to occlusion.

In addition to the L2 norm loss  $\mathcal{L}_{3D}$ , we employ a silhouette loss  $\mathcal{L}_s$  which counts the number of predicted body surface points whose projections fall outside of the 2D rat region in a view [17]

$$\mathcal{L}_s = \sum_{n=1}^N M_c(P_c(\mathbf{x}_n)), \quad (1)$$

where  $P_c$  is a projection function onto the view  $c$  and  $M_c$  is a mask image of view  $c$ .  $M_c(\mathbf{v})$  is a pixel value of  $M_c$  at the image coordinate  $\mathbf{v}$ .

**Semi-Automatic Annotation** RatDome Dataset contains many frames capturing color-beaded rats but without manual annotations (Sec. 3.1). We derive a semi-supervised learning method to make full use of this data. The method leverages a small number of frames fully-annotated with ground-truth to infer the labels for the remaining frames. First, we compute the 3D coordinates of the markers. This process is automated, similar to that of the Panoptic Studio Dataset [22]. We detect the 2D markers from each image with an object detector [13] trained with manual annotations. We then leverage multiview triangulation to disambiguate markers of the same color on the body surface.

Once the 3D marker coordinates are computed for each frame, we assign their marker IDs so that they are consistent with the manually annotated ones by using RatBodyFormer itself. Suppose we have trained RatBodyFormer using only the manually-annotated frames. We use this initial model to estimate the 3D coordinates of the body surface points, and find the correspondences between the triangulated 3D points and those estimated by RatBodyFormer by minimizing their Euclidean distance [26]. These correspondences allow transfer of marker IDs from the manually annotated body surface points to the automatically triangulated body surface points so that RatBodyFormer can be retrained using both the manually-annotated and automatically-annotated frames. We define this automatically-annotated labels as the *semi-automatically annotated labels* to distinguish them from manually annotated labels. We experimentally show that the use of semi-automatically annotated labels improve estimation accuracy (Sec. 4.2).

**Training** The input parameters of RatBodyFormer are the keypoint coordinates  $\mathbf{P}$ , the individual-dependent scaling factors  $\mathbf{C} = \{\mathbf{C}_P, \mathbf{C}_B\}$ , and translations  $\mathbf{T} = \{\mathbf{T}_P, \mathbf{T}_B\}$ . We alternate between the optimization of RatBodyFormer and the individual-dependent parameters. The individual-dependent  $\mathbf{C}$  and  $\mathbf{T}$  are initialized by  $\alpha$ s and 0s, respectively. Here  $\alpha$  is obtained as a result of aligning the canonical 3D body surface  $\hat{S}$  as mentioned before. At every epoch of the training, we optimize RatBodyFormer by minimizing  $\mathcal{L}_{3D}$ , while keeping the individual-dependent parameters fixed. During this optimization, we refine  $\mathbf{C}$  and  $\mathbf{T}$  by optimizing  $\mathcal{L}_s$  at every  $T$  epochs, while keeping RatBodyFormer fixed. We use  $T = 50$  in our experiments.

**Inference** We estimate the scaling and translation parameters  $\mathbf{C}$  and  $\mathbf{T}$  of a new rat with inference-time optimization using the silhouette loss  $\mathcal{L}_s$ . The initial value  $\alpha_p$  for  $\mathbf{C}_P$  and  $\alpha_B$  for  $\mathbf{C}_B$  are manually set by the ratio of the length from the nose to the base of tail, and the ratio of the girth length, respectively. After optimizing  $\mathbf{C}$  and  $\mathbf{T}$ , we regress the body surface point coordinates.

## 4. Experiments

We evaluate the effectiveness of RatBodyFormer with a number of experiments each focused on validating key properties of them. First, in Sec. 4.2, we evaluate the accuracy and generalizability of RatBodyFormer. Next, in Sec. 4.3, we demonstrate future 3D body surface prediction by forecasting with RatBodyFormer.

### 4.1. RatDome and RatDome Dataset

RatDome is equipped with 15 GoPro 10 cameras and 5 Intel L515 LiDAR-Camera devices. The LiDAR cameras are installed for potential ground truth measurements. We found that the depth captured with the LiDAR cameras were noisy and have too many holes for any direct measurement. We only use the depth images for D3 of Sec. 4.2 by combining it with shape-from-silhouette. GoPro captures 4K videos at 60Hz, and L515 captures 1080p videos at 30Hz and 1024×768 depthmaps at 30Hz. We place a translucent acrylic tube of 300mm diameter and 5mm thick as a rat cage to avoid the rat from moving into the corners.

All the cameras are calibrated by capturing a chessboard moved around in the dome. The mean reprojection error after regular bundle adjustment was about 1.1 pixels [18]. Refraction by the acrylic tube is not modeled in the camera calibration. The cameras are temporally synchronized with flash light from a strobe.

### 4.2. RatBodyFormer

We evaluate the accuracy of RatBodyFormer in different scenarios. We first train and test the model using a single rat where the training and the testing sets share the same

Split	Test	Val	Train	
	MA	MA	MA	SAA
D1	7w p1	7w p2	7w p3-12	7w
D2	7w/11w p1	7w/11w p2	7w/11w p3-12	7w,11w
D3	-	7w/11w p11	7w/11w p1-10,12	7w, 9w, 11w

Table 1. Our RatDome Dataset split for evaluation. “w” and “p” mean “week-old” and “part”, respectively. “MA” and “SAA” are annotation types, and mean “manually-annotated data” and “semi-automatically annotated data”, respectively.

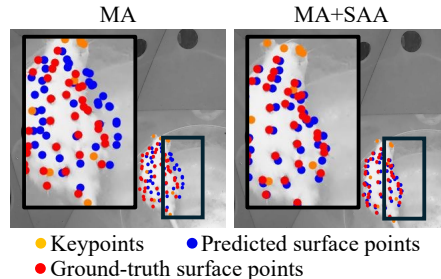


Figure 5. Qualitative results of D1. We show the results of trained by only manually-annotated data (MA) in the left, and the results of trained by manually-annotated and semi-automatically annotated data (SAA) in the right. Semi-automatically annotated data improve the body surface estimation.

marker annotations (D1). We specifically evaluate the advantage of using semi-automatically annotated labels, the frames automatically annotated with RatBodyFormer itself (Sec. 3.2). Next, we combine two rats of different ages of weeks for training and testing (D2). This experiment quantifies the advantage of learning across individual rats. Finally, we use the entire RatDome Dataset, where we can use 7, 9, and 11 week-old annotations for training (D3), and use 5 and 14 week-old rats without markers to evaluate the generalizability of the proposed method.

Tab. 1 summarizes the dataset splits for these evaluations, D1, D2, and D3. We divide the manually annotated data of 7, 11 week-olds into 12 parts in a temporally sequential order, one for testing, one for validation, and the rest for training. Because our semi-automatically annotated labels sometimes mistake surface marker IDs, we use semi-automatically annotated data only for training.

**D1: Single Rat** Fig. 6 shows the L2 error histograms for D1 between the predicted body surface 3D coordinates and the corresponding manually-annotated ground truths. This result demonstrates the advantage of using semi-automatically annotated labels as they improve the accuracy by about 1.7 mm. Fig. 5 shows qualitative results.

**D2: Two Rats** Fig. 8 shows the results for D2. For this cross-individual experiments, the semi-automatically anno-

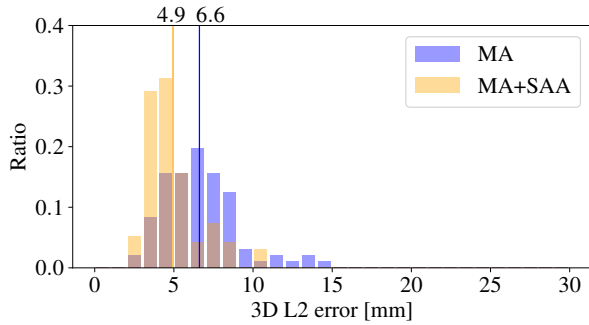


Figure 6. L2 error histograms of D1. Each vertical bar indicates the mean L2 error of the histogram in the same color. Our semi-automatically annotation label improve average error by about 1.7 mm. “MA” and “SAA” mean “manually-annotated data”, and “semi-automatically annotated data”, respectively.

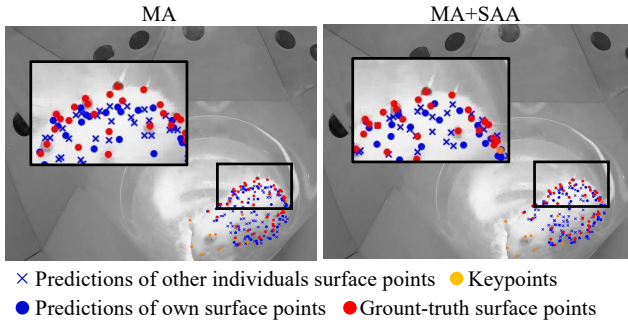


Figure 7. Qualitative results of D2. The left represents the results trained by only manually-annotated data (MA), and the right row shows the result of manually and semi-automatically annotated data (SAA). Our semi-automatically annotated labels also improve the quality in this scenario.

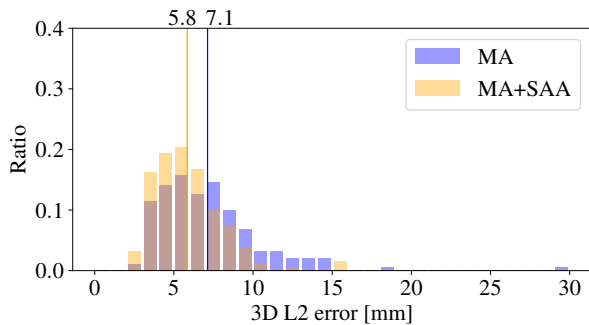


Figure 8. L2 error histograms of D2. Each vertical bar indicates the mean L2 error of the histogram in the same color. “MA” and “SAA” mean “manually-annotated data” and “semi-automatically annotated data”, respectively. Our semi-automatically annotated data improve L2 error by about 1.3mm.

tation labels also improve the accuracy. Fig. 7 shows qualitative results.

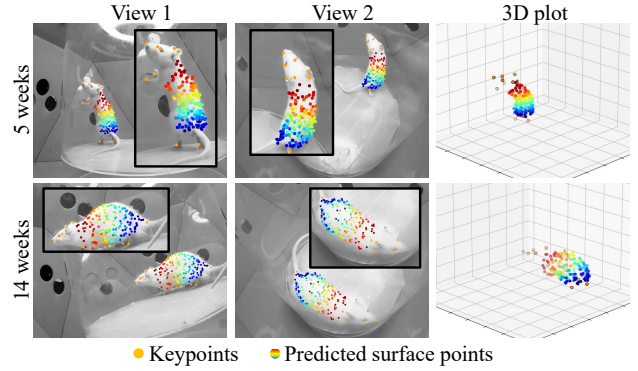


Figure 9. Qualitative results of D3. The first row and the second row show the estimated surface points for the 5 and 14 week-olds, respectively. The left and the center images show a single frame from different views. The right image shows the 3D keypoints and the 3D predicted surface points. The predicted surface points are on the rat surface.

**D3: All Rats** In this scenario, we train the model using 7, 9, and 11 week-old rats with the manually-annotated and semi-automatically annotated data and evaluate the accuracy on the 5 and 14 week-old rats without markers. For this, we define ground-truth surface points as the sum of the set of points captured by LiDAR and shape-from-silhouette. As many of the LiDAR points have missing values and errors, we add surface points obtained by shape-from-silhouette. We optimize individual-dependent parameters  $C$  and  $T$  with the silhouette loss Eq. (1). We obtain the mask images with SAM [24, 41]. The average estimation errors for 5 and 14 week-old rats are 3.98 mm and 6.39 mm, respectively. Note that we calculate only the dorsal side surface points because the ventral side sometimes occluded. Our model can estimate any shape of rat even if individuals not included in the training data. Fig. 9 shows the estimated body surface points. The results show that RatBodyFormer can be applied to a variety of rats ranging from 5 to 14 week-olds. This covers the age range typically used in biomedical and neuroscientific experiments.

### 4.3. Pose Forecasting

In this section, we show that our surface model can predict future rat 3D body surface by just predicting detectable keypoint coordinates. As shown in Fig. 11, we train a transformer-based auto-regressive 3D keypoints prediction model. The input of this model is a sequence of keypoint 3D coordinates for past  $\tau_p$  frames, and the output is the 3D keypoint coordinates of the next  $\tau_n$  frames. We trained the model with 5, 7, 9, 11, and 14 week-old data for about 10000 frames in total and tested with 7 week-old data for about 500 frames.

Fig. 12 shows the histogram of L2 errors in the pre-

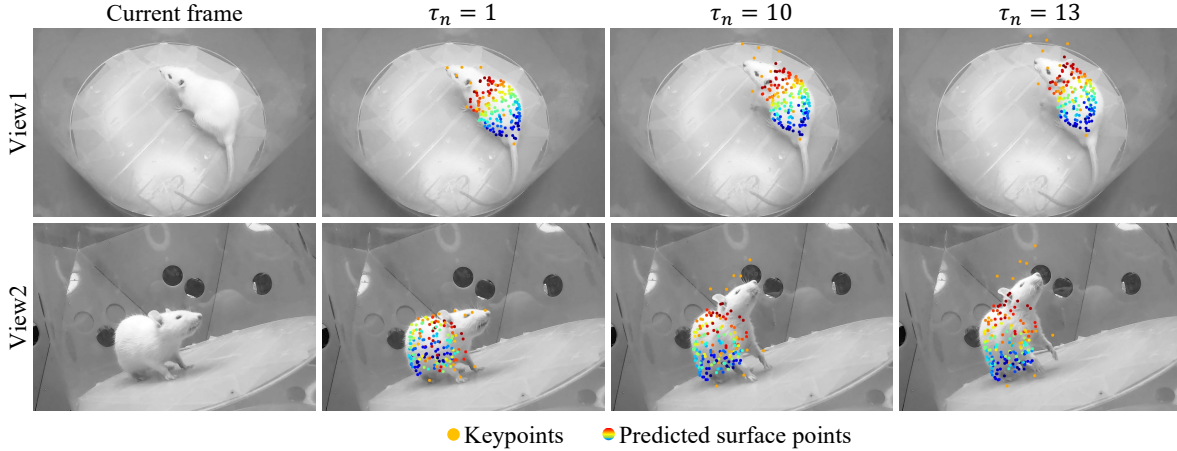


Figure 10. Future rat body pose estimation. We take keypoint 3D coordinates for  $\tau_p = 3$  frames as input, and estimate  $\tau_n = 1, 10, 13$  future pose with the pose forecasting model and our RatBodyFormer. We can forecast future body poses by just predicting future keypoints. The accuracy degrades gracefully as we forecast further into the future.

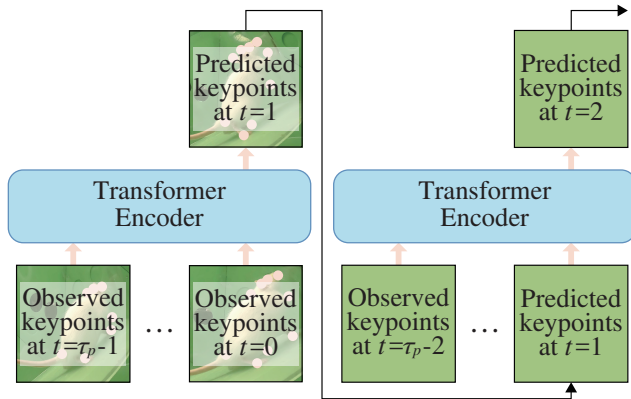


Figure 11. Transformer encoder for keypoint forecasting. The input is a sequence of past concatenated  $K = 10$  keypoint 3D coordinates, and the output is 3D keypoint coordinates of the next frame. It predicts future keypoints’ coordinates auto-regressively.

dicted keypoints at  $\tau_p = 3$  and  $\tau_n = 1, 3, 5$  frames. At  $\tau_n = 1$ , our model can predict the future keypoint positions in most cases accurately, except for when the rat goes under rapid movements, such as suddenly changing directions. We leave investigation of more sophisticated methods for complex motion prediction as future work. Fig. 10 shows predictions of the body surface points by RatBodyFormer. Given predicted 3D keypoint coordinates in the future frames, RatBodyFormer can infer the 3D body surface coordinates from them. This is possible as RatBodyFormer effectively reduces the necessary points for forecasting to those that are well-defined. We believe this forecasting scheme can benefit a wide-range of scientific experiments, especially that concern multiple rats.

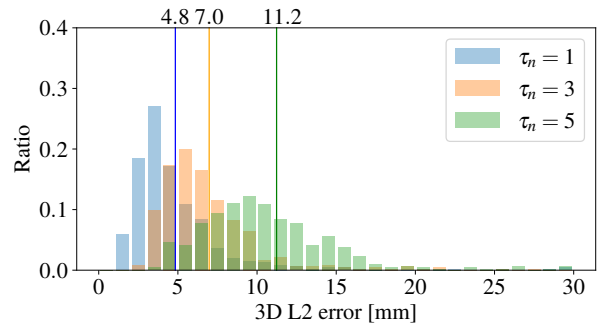


Figure 12. Histogram of 3D keypoint prediction errors. Each vertical bar indicates the mean L2 error of the histogram in the same color. As the peak average error at  $\tau_p = 1$  is about 3mm, we can predict 3D keypoint coordinates in most cases. Since errors accumulate, the larger  $\tau_n$  is, the bigger its error is.

## 5. Conclusion

This paper proposed the RatDome Dataset and RatBodyFormer. The RatDome Dataset is the first-of-its-kind dataset which provides 3D body surface coordinates with temporally-consistent annotations from 7, 9, and 11 week-old rats. RatBodyFormer models the highly nonrigid deformation of the rat body and can regress the body surface 3D coordinates from its keypoint 3D coordinates. Experimental results demonstrated that RatBodyFormer can generalize to model the body surface points of 5 and 14 week-old rats which are not included in the training dataset.

We believe that our RatDome Dataset and RatBodyFormer collectively serve a novel, sound foundation for autonomous rat behavior analysis and will likely have far-reaching implications for biomedical and neuroscientific research.



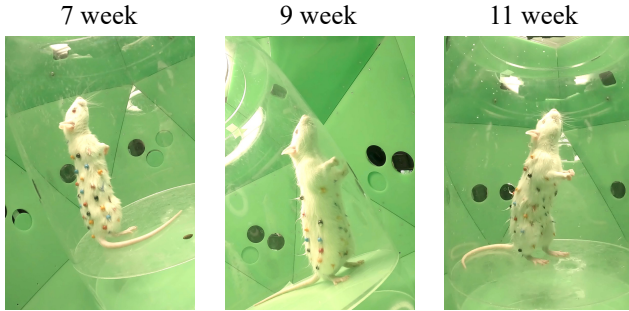


Figure A. Manually selected standing-on-two-feet poses of 7-, 9-, 11-week-old rats. All of the markers are visible from the cameras.

## Acknowledgements

This work was in part supported by JSPS 20H05951, 21H04893, 23H04336, and 24H01544, AMED 24wm0625401h0001, JST JPMJPR22S8, JPMJCR20G7, and JPMJAP2305, the Secom Science and Technology Foundation and RIKEN GRP.

## A. Implementation Details of Canonical Body Surface

As shown in Fig. A, we first manually select a similar pose from each individual rat to map the marker positions to a common canonical body surface. To this end, we selected a standing-on-two-feet pose in which all the markers are visible from the cameras. Given these selected poses, we used the 7-week-old as the reference, and aligned the others by a similarity transform and ARAP deformation as follows.

We first normalized their scales, positions, and orientations by applying a similarity transform estimated from their keypoint positions. After this similarity transform, the keypoints and surface points are aligned with ARAP deformation using the keypoints as its hard constraints and surface points as its soft constraints. The target position used in the soft constraint for each surface point is chosen as the point on the visual hull of the target rat closest from the surface point in each ARAP iteration.

## B. Evaluations with Other Data Splits

To demonstrate the generalizability of our RatBodyFormer, we further evaluate the accuracy of RatBodyFormer with other data splits. Tab. A shows the dataset splits of D1 and D2 scenarios. The splits “D1” and “D2” in Table 1 of the main paper appear as D1-a and D2-a in this table, respectively.

**D1: Single Rat** Fig. B (a), (b), and (c) show the error histograms of D1-b, D1-c, and D1-d, respectively.

Split	Test	Val	Train	SAA
	MA	MA	MA	
D1-a	7w p1	7w p2	7w p3-12	7w
D1-b	7w p12	7w p11	7w p1-10	7w
D1-c	11w p1	11w p2	11w p3-12	11w
D1-d	11w p12	11w p11	11w p1-10	11w
D2-a	7w/11w p1	7w/11w p2	7w/11w p3-12	7w,11w
D2-b	7w/11w p12	7w/11w p11	7w/11w p1-10	7w,11w

Table A. Our RatDome Dataset split for evaluation. “w” and “p” stand for “week-old” and “part”, respectively. “MA” and “SAA” are annotation types, and stand for “manually-annotated data” and “semi-automatically annotated data”, respectively.

Fig. C shows qualitative results of these splits. Our semi-automatically annotated data improve accuracy in all these splits consistently.

**D2: Two Rats** Fig. D shows the error histogram of D2-b and Fig. E shows qualitative results. These results demonstrate quantitatively and qualitatively that our semi-automatically annotated data improves accuracy regardless of the dataset splits.

## C. Ablation Study

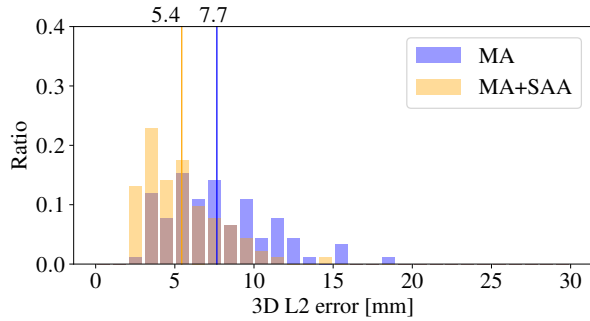
### C.1. Individual-dependent Parameters

This section evaluates the effect of the individual-dependent parameters, *i.e.*, point-wise scaling parameters  $\mathbf{C}$  and translation parameters  $\mathbf{T}$  for the training time and inference time. Fig. F evaluates the contribution of optimizing the individual-dependent parameters at training time using D2-a and D2-b splits. For the case of training without optimizing individual-dependent parameters, we set  $\mathbf{C} = 1$  and  $\mathbf{T} = 0$ . These results show that optimizing the individual-dependent parameters at training time improves the estimation accuracy.

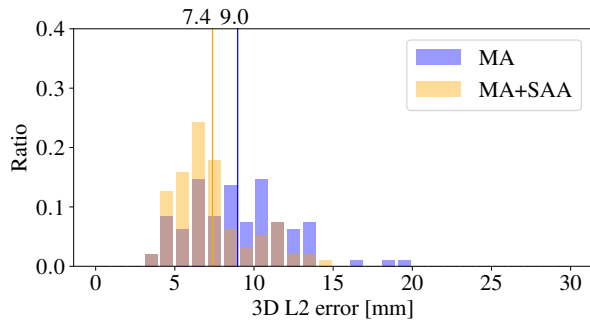
Fig. G shows the effect of optimizing the individual-dependent parameters at inference time using the D3 split in Table 1 of the main text. In this split, RatBodyFormer is trained using 7-, 9-, and 11-week-old rats with manually-annotated and semi-automatically annotated data, and evaluated with 5- and 14-week-old rats using 3D points obtained by LiDAR and shape-from-silhouette as described in the main text. For the results of inference without optimizing individual-dependent parameters, we set  $\mathbf{C} = 1$  and  $\mathbf{T} = 0$ . We can observe that the inference time optimization clearly improves the estimation accuracy.

### C.2. Data Normalization

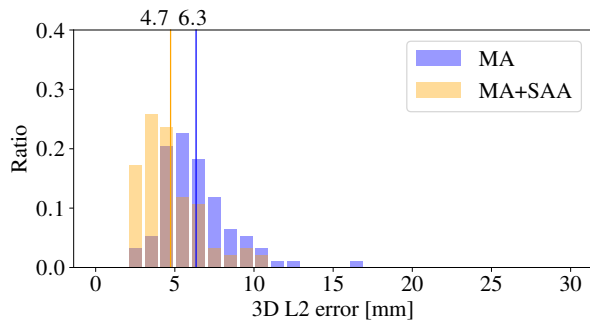
Fig. H shows the effect of our data normalization applied to the input of RatBodyFormer described in L283 of the main text using D1 splits. These results clearly demonstrates that the normalization significantly improves the accuracy.



(a) L2 error histogram of D1-b



(b) L2 error histogram of D1-c



(c) L2 error histogram of D1-d

Figure B. L2 error histograms of D1-b, D1-c, and D1-d. Each vertical bar indicates the mean L2 error of the histogram in the same color. “MA” and “SAA” denote “manually-annotated data”, and “semi-automatically annotated data”, respectively. Our semi-automatically annotated data improves accuracy by 1.6 mm to 2.3 mm.

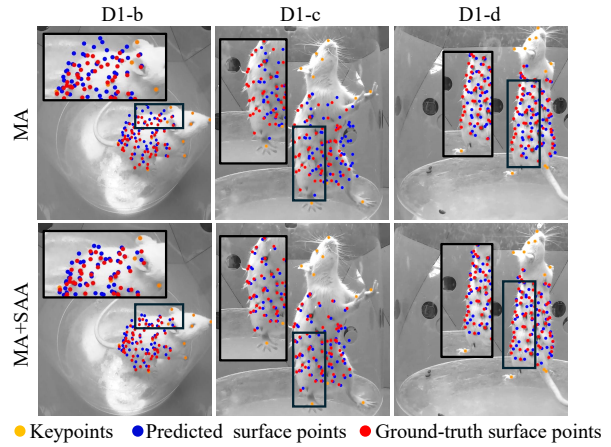


Figure C. Qualitative results of D1-b, D1-c, and D1-d. We show the results of only using manually-annotated data (MA) for training in the top row, and the results of also using semi-automatically annotated data (SAA) for training in the bottom row. The addition of semi-automatically annotated data improves the body surface estimation.

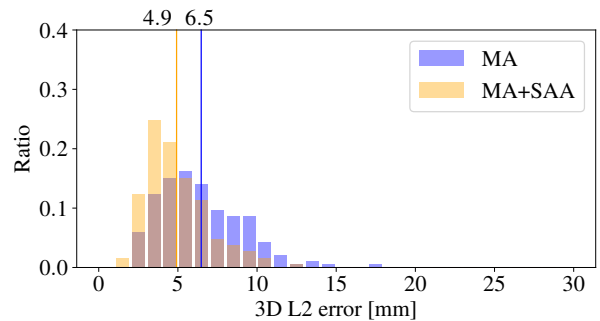


Figure D. L2 error histogram of D2-b. Each vertical bar indicates the mean L2 error of the histogram in the same color. “MA” and “SAA” represent “manually-annotated data”, and “semi-automatically annotated data”, respectively. The semi-automatically annotated data improves average error by about 1.6 mm.

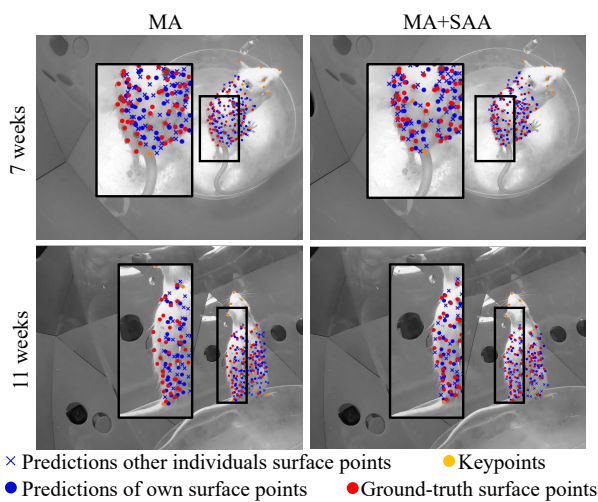
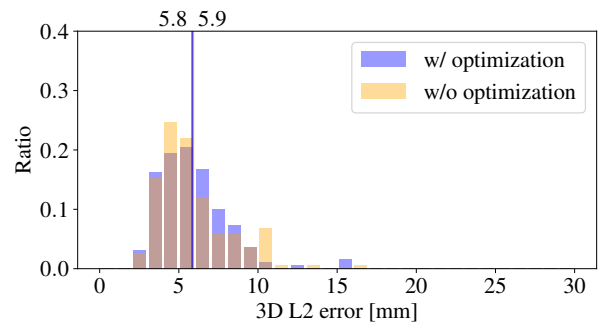
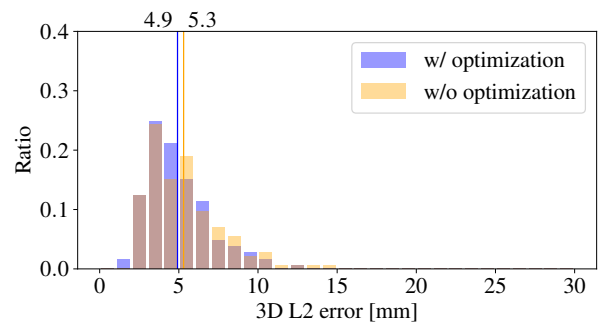


Figure E. Qualitative results of D2-b. We show the results of RatBodyFormer trained with only manually-annotated data (MA) in the left, and that trained with both manually-annotated and semi-automatically annotated data (SAA) in the right. Semi-automatically annotated data clearly improves the body surface estimation.

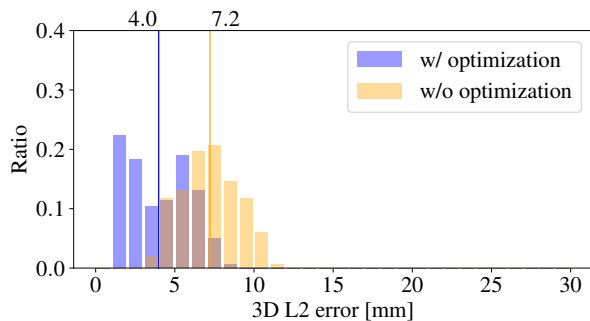


(a) L2 error histogram of D2-a

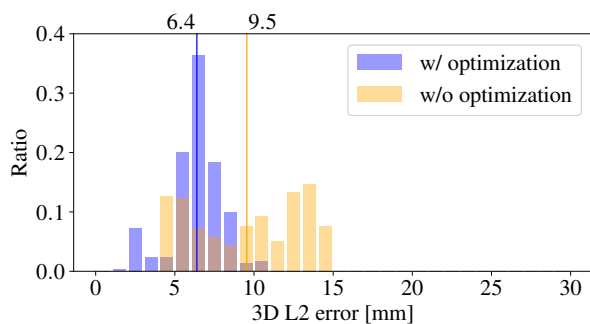


(b) L2 error histogram of D2-b

Figure F. L2 error histograms of D2-a and D2-b. Each vertical bar shows the mean L2 error of the histogram in the same color. The blue and orange histograms show the errors with and without optimizing the individual-dependent parameters, respectively. Training with individual-dependent parameter optimization consistently improves the estimation accuracy.

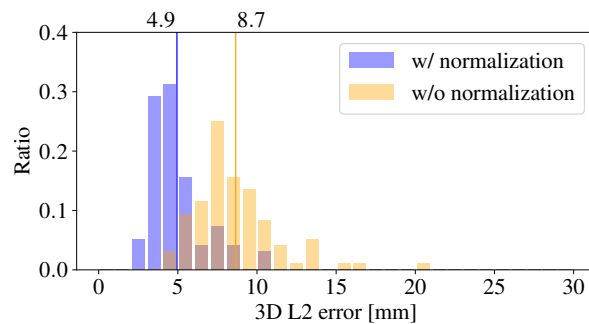


(a) L2 error histogram of 5 week old

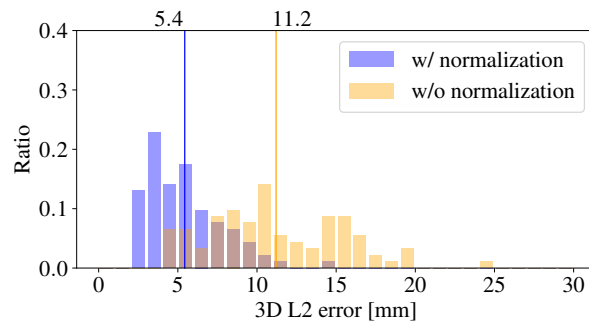


(b) L2 error histogram of 14 week old

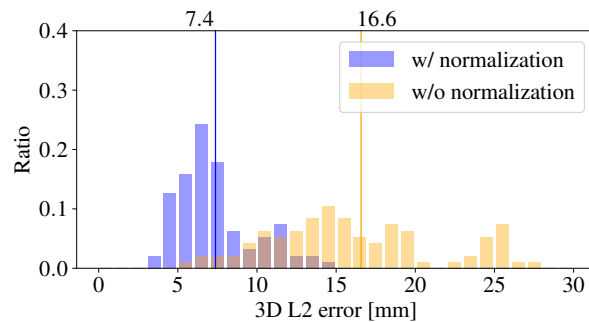
Figure G. L2 error histograms of 5- and 14-week-old rats. Each vertical bar indicates the mean L2 error of the histogram in the same color. The blue and orange histograms show the errors with and without optimizing the individual-dependent parameters, respectively. Inference-time optimization of the individual-dependent parameters consistently improves the estimation accuracy.



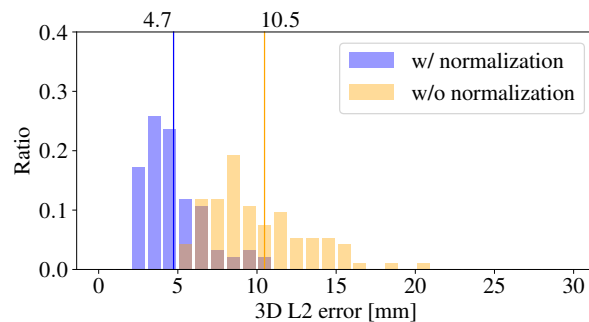
(a) L2 error histogram of D1-a



(b) L2 error histogram of D1-b



(c) L2 error histogram of D1-c



(d) L2 error histogram of D1-d

Figure H. L2 error histograms of D1-a, D1-b, D1-c, and D1-d. Each vertical bar shows the mean L2 error of the histogram in the same color. Our data normalization improves the average L2 error by about 3.8 mm to 9.2 mm.

## References

- [1] Alexander Mathis, Pranav Mamidanna, Kevin M. Cury, Taiga Abe, Venkatesh N. Murthy, Mackenzie Weygandt Mathis, and Matthias Bethge. DeepLabCut: markerless pose estimation of user-defined body parts with deep learning. *Nature Neuroscience*, pages 1281–1289, 2018. 2, 3
- [2] Serge Belongie, Kristin Branson, Piotr Dollár, and Vincent Rabaud. Monitoring Animal Behavior in the Smart Vivarium. In *Measuring Behavior*, pages 70–72, 2005. 2
- [3] Dan Biderman, Matthew R. Whiteway, Cole Hurwitz, Nicholas Greenspan, Robert S. Lee, Ankit Vishnubhotla, Richard Warren, Federico Pedraja, Dillon Noone, Michael M. Schartner, Julia M. Huntentburg, Anup Khanal, Guido T. Meijer, Jean-Paul Noel, Alejandro Pan-Vazquez, Karolina Z. Socha, Anne E. Urai, The International Brain Laboratory, John P. Cunningham, Nathaniel B. Sawtell, and Liam Paninski. Lightning Pose: improved animal pose estimation via semi-supervised learning, Bayesian ensembling and cloud-native open-source tools. *Nature Neuroscience*, pages 1316–1328, 2024. 2
- [4] Federica Bogo, Angjoo Kanazawa, Christoph Lassner, Peter Gehler, Javier Romero, and Michael J. Black. Keep it SMPL: Automatic Estimation of 3D Human Pose and Shape from a Single Image. In *ECCV*, pages 561–578, 2016. 3
- [5] James P Bohnslav, Mohammed Abdal Monium Osman, Akshay Jaggi, Sofia Soares, Caleb Weinreb, Sandeep Robert Datta, and Christopher D Harvey. ArMo: An Articulated Mesh Approach for Mouse 3D Reconstruction. *BioRxiv*, 2023. 2
- [6] Zhe Cao, Tomas Simon, Shih-En Wei, and Yaser Sheikh. Realtime Multi-Person 2D Pose Estimation using Part Affinity Fields. In *CVPR*, pages 7291–7299, 2017. 2
- [7] Fabrice Chaumont, Renata Coura, Pierre Serreau, Arnaud Cressant, Jonathan Chabout, Sylvie Granon, and Jean-Christophe Olivo-Marin. Computerized video analysis of social interactions in mice. *Nature Methods*, pages 410–417, 2012. 2
- [8] Sandeep Robert Datta, David J. Anderson, Kristin Branson, Pietro Perona, and Andrew Leifer. Computational Neuroethology: A Call to Action. *Neuron*, pages 11–24, 2019. 2
- [9] Anthony I. Dell, John A. Bender, Kristin Branson, Iain D. Couzin, Gonzalo G. de Polavieja, Lucas P.J.J. Noldus, Alfonso Pérez-Escudero, Pietro Perona, Andrew D. Straw, Martin Wikelski, and Ulrich Brose. Automated image-based tracking and its application in ecology. *Trends in Ecology and Evolution*, pages 417–428, 2014. 2
- [10] Timothy W Dunn, Jesse D Marshall, Kyle S Severson, Diego E Aldarondo, David GC Hildebrand, Selmaan N Chetih, William L Wang, Amanda J Gellis, David E Carlson, Dmitriy Aronov, et al. Geometric deep learning enables 3D kinematic profiling across species and environments. *Nature Neuroscience*, pages 564–573, 2021. 2
- [11] Christian L Ebbesen and Robert C Froemke. Body language signals for rodent social communication. *Current Opinion in Neurobiology*, pages 91–106, 2021. 3
- [12] S.E. Roian Egnor and Kristin Branson. Computational Analysis of Behavior. *Neuroscience and Biobehavioral Reviews*, pages 217–236, 2016. 2
- [13] Zheng Ge, Songtao Liu, Feng Wang, Zeming Li, and Jian Sun. YOLOX: Exceeding YOLO Series in 2021. *arXiv:2107.08430*, 2021. 5
- [14] Adam Gosztolai, Semih Günel, Marco Pietro Abrate, Daniel Morales, Victor Ríos, Helge Rhodin, Pascal Fua, and Pavan Ramdya. LiftPose3D, a deep learning-based approach for transforming 2D to 3D pose in laboratory animals. *Nature Methods*, pages 975–981, 2021. 2
- [15] Evan H. Goulding, A. Katrin Schenk, Punita Juneja, Adrienne W. MacKay, Jennifer M. Wade, and Laurence H. Tecott. A robust automated system elucidates mouse home cage behavioral structure. *Proceedings of the National Academy of Sciences*, pages 20575–20582, 2008. 2
- [16] Rıza Alp Güler, Natalia Neverova, and Iasonas Kokkinos. DensePose: Dense Human Pose Estimation in the Wild. In *CVPR*, pages 7297–7306, 2018. 3
- [17] Zhizhong Han, Chao Chen, Yu-Shen Liu, and Matthias Zwicker. DRWR: A differentiable renderer without rendering for unsupervised 3D structure learning from silhouette images. In *ICML*, pages 3994–4005, 2020. 5
- [18] Richard Hartly and Andrew Zisserman. *Multiple view geometry in computer vision*. 2004. 6
- [19] Bo Hu, Bryan Seybold, Shan Yang, Avneesh Sud, Yi Liu, Karla Barron, Paulyn Cha, Marcelo Cosino, Ellie Karlsson, Janessa Kite, Ganesh Kolumam, Joseph Preciado, José Zavala-Solorio, Chunlian Zhang, Xiaomeng Zhang, Martin Voorbach, Ann E. Tovicimak, J. Graham Ruby, and David A. Ross. 3D mouse pose from single-view video and a new dataset. *Scientific Reports*, pages 2045–2322, 2023. 2
- [20] Buzhen Huang, Yuan Shu, Tianshu Zhang, and Yangang Wang. Dynamic Multi-Person Mesh Recovery From Uncalibrated Multi-View Cameras. In *3DV*, pages 710–720. IEEE, 2021. 3
- [21] Yinghao Huang, Federica Bogo, Christoph Lassner, Angjoo Kanazawa, Peter V Gehler, Javier Romero, Ijaz Akhter, and Michael J Black. Towards accurate marker-less human shape and pose estimation over time. In *3DV*, pages 421–430, 2017. 3
- [22] Hanbyul Joo, Hao Liu, Lei Tan, Lin Gui, Bart Nabbe, Iain Matthews, Takeo Kanade, Shohei Nobuhara, and Yaser Sheikh. Panoptic Studio: A Massively Multiview System for Social Motion Capture. In *ICCV*, pages 3334–3342, 2015. 3, 5
- [23] Angjoo Kanazawa, Michael J. Black, David W. Jacobs, and Jitendra Malik. End-to-end Recovery of Human Shape and Pose. In *CVPR*, 2018. 3
- [24] Alexander Kirillov, Eric Mintun, Nikhila Ravi, Hanzi Mao, Chloe Rolland, Laura Gustafson, Tete Xiao, Spencer Whitehead, Alexander C. Berg, Wan-Yen Lo, Piotr Dollar, and Ross Girshick. Segment Anything. In *ICCV*, pages 4015–4026, 2023. 7
- [25] Nikos Kolotouros, Georgios Pavlakos, Michael J Black, and Kostas Daniilidis. Learning to reconstruct 3D human pose and shape via model-fitting in the loop. In *ICCV*, pages 2252–2261, 2019. 3

- [26] Harold W Kuhn. The Hungarian method for the assignment problem. *Naval research logistics quarterly*, pages 83–97, 1955. 5
- [27] Bruno Lévy. Laplace-beltrami eigenfunctions towards an algorithm that “understands” geometry. In *IEEE International Conference on Shape Modeling and Applications*, pages 13–13, 2006. 5
- [28] Tianye Li, Timo Bolkart, Michael J. Black, Hao Li, and Javier Romero. Learning a model of facial shape and expression from 4D scans. *ACM Transactions on Graphics*, pages 194:1–194:17, 2017. 3
- [29] Zizhang Li, Dor Litvak, Ruining Li, Yunzhi Zhang, Tomas Jakab, Christian Rupprecht, Shangzhe Wu, Andrea Vedaldi, and Jiajun Wu. Learning the 3D Fauna of the Web. In *CVPR*, pages 9752–9762, 2024. 3
- [30] Matthew Loper, Naureen Mahmood, Javier Romero, Gerard Pons Moll, and Michael J. Black. SMPL: A Skinned Multi-Person Linear Model. *ACM Transactions on Graphics*, pages 248:1–248:16, 2015. 3, 4
- [31] Malte Lorbach, Elisavet I. Kyriakou, Ronald Poppe, Elisabeth A. van Dam, Lucas P.J.J. Noldus, and Remco C. Veltkamp. Learning to recognize rat social behavior: Novel dataset and cross-dataset application. *Journal of Neuroscience Methods*, pages 166–172, 2018. 2
- [32] Omid Haji Maghsoudi, Annie Vahedipour Tabrizi, Benjamin Robertson, and Andrew Spence. Superpixels Based Marker Tracking Vs. Hue Thresholding In Rodent Biomechanics Application. *arXiv:1710.06473*, 2017. 2
- [33] Jesse D. Marshall, Diego E. Aldarondo, Timothy W. Dunn, William L. Wang, Gordon J. Berman, and Bence P. Ölveczky. Continuous Whole-Body 3D Kinematic Recordings across the Rodent Behavioral Repertoire. *Neuron*, pages 420–437, 2021. 2
- [34] Julieta Martinez, Rayat Hossain, Javier Romero, and James J. Little. A Simple yet Effective Baseline for 3D Human Pose Estimation. In *ICCV*, pages 2640–2649, 2017. 2
- [35] Jumpei Matsumoto, Susumu Urakawa, Yusaku Takamura, Renato Malcher-Lopes, Etsuro Hori, Carlos Tomaz, Take-toshi Ono, and Hisao Nishijo. A 3D-Video-Based Computerized Analysis of Social and Sexual Interactions in Rats. *PLoS One*, page e78460, 2013. 2
- [36] Bartul Mimica, Benjamin A. Dunn, Tuce Tombaz, V. P. T. N. C. Srikanth Bojja, and Jonathan R. Whitlock. Efficient cortical coding of 3D posture in freely behaving rats. *Science*, pages 584–589, 2018. 2
- [37] Mate Nagy, Jacob D. Davidson, Gabor Vasarhelyi, Daniel Abel, Eniko Kubinyi, Ahmed El Hady, and Tamas Vicsek. Long-term tracking of social structure in groups of rats. *arXiv:2408.08945*, 2024. 2
- [38] Natalia Neverova, David Novotny, Marc Szafranec, Vasil Khalidov, Patrick Labatut, and Andrea Vedaldi. Continuous Surface Embeddings. In *NeurIPS*, pages 17258–17270, 2020. 3, 5
- [39] T. D. Pereira, D. E. Aldarondo, L. Willmore, M. Kislin, S. S. Wang, M. Murthy, and J. W. Shaevitz. Fast animal pose estimation using deep neural networks. *Nature Neuroscience*, pages 117–125, 2019. 2
- [40] Leonid Pishchulin, Eldar Insafutdinov, Siyu Tang, Bjoern Andres, Mykhaylo Andriluka, Peter V. Gehler, and Bernt Schiele. DeepCut: Joint Subset Partition and Labeling for Multi Person Pose Estimation. In *CVPR*, pages 4929–4937, 2016. 2
- [41] Nikhila Ravi, Valentin Gabeur, Yuan-Ting Hu, Ronghang Hu, Chaitanya Ryali, Tengyu Ma, Haitham Khedr, Roman Rädle, Chloe Rolland, Laura Gustafson, Eric Mintun, Junting Pan, Kalyan Vasudev Alwala, Nicolas Carion, Chao-Yuan Wu, Ross Girshick, Piotr Dollár, and Christoph Feichtenhofer. SAM 2: Segment Anything in Images and Videos. *arXiv:2408.00714*, 2024. 7
- [42] Remy Sabathier, Niloy Jyoti Mitra, and David Novotny. Animal Avatars: Reconstructing Animatable 3D Animals from Casual Videos. *arXiv:2403.17103*, 2024. 3
- [43] Olga Sorkine and Marc Alexa. As-Rigid-As-Possible Surface Modeling. In *Symposium on Geometry processing*, pages 109–116, 2007. 4, 5
- [44] Ashish Vaswani, Noam Shazeer, Niki Parmar, Jakob Uszkoreit, Llion Jones, Aidan N Gomez, Łukasz Kaiser, and Illia Polosukhin. Attention is All you Need. In *NeurIPS*, pages 5998–6008, 2017. 4
- [45] Gengshan Yang, Minh Vo, Natalia Neverova, Deva Ramanan, Andrea Vedaldi, and Hanbyul Joo. BANMO: Building Animatable 3D Neural Models From Many Casual Videos. In *CVPR*, pages 2863–2873, 2022. 3
- [46] Shaokai Ye, Anastasiia Filippova, Jessy Lauer, Steffen Schneider, Maxime Vidal, Tian Qiu, Alexander Mathis, and Mackenzie Weygandt Mathis. Superanimal pretrained pose estimation models for behavioral analysis. *Nature Communications*, page 5165, 2024. 2, 4
- [47] Kim Youwang, Kim Ji-Yeon, Kyungdon Joo, and Tae-Hyun Oh. Unified 3D Mesh Recovery of Humans and Animals by Learning Animal Exercise. *BMVC*, 2021. 3
- [48] Christian Zimmermann, Artur Schneider, Mansour Alyahyay, Thomas Brox, and Ilka Diester. FreiPose: a deep learning framework for precise animal motion capture in 3D spaces. *BioRxiv*, pages 2020–02, 2020. 2
- [49] Silvia Zuffi, Angjoo Kanazawa, David W. Jacobs, and Michael J. Black. 3D Menagerie: Modeling the 3D Shape and Pose of Animals. In *CVPR*, pages 6365–6373, 2017. 3, 4
- [50] Silvia Zuffi, Angjoo Kanazawa, Tanya Berger-Wolf, and Michael J Black. Three-D Safari: Learning to Estimate Zebra Pose, Shape, and Texture from Images “In the Wild”. In *CVPR*, pages 5359–5368, 2019. 3
- [51] Silvia Zuffi, Ylva Mellbin, Ci Li, Markus Hoeschle, Hedvig Kjellström, Senya Polikovsky, Elin Hernlund, and Michael J. Black. VAREN: Very Accurate and Realistic Equine Network. In *CVPR*, pages 5374–5383, 2024. 3, 4